Sains Malaysiana 55(7)(2026): 1198-1210
http://doi.org/10.17576/jsm-2026-5507-08

Physicochemical Characteristics of Hydroxyapatite/Beta-Tricalcium Phosphate from *Pinctada maxima* Shells for Resorbable Bone Matrix Candidate

(Ciri Fizikokimia Hidroksiapatit/Beta-Trikalsium Fosfat daripada Cangkerang *Pinctada maxima* untuk Calon Matriks Tulang Boleh Serap)

AHMAD TAUFIK S[1,*], SUSI RAHAYU[2,3], MOHAMMAD RIZKI[1], M. MUKADDAM ALAYDRUS[1], I GUSTI AYU SRI ANDAYANI[1], IRNAWATI[2] & MUHAMAD ALI[4]

[1]*Department of Medical Sciences, Faculty of Medicine and Health Sciences, University of Mataram, Mataram, 83125, West Nusa Tenggara, Indonesia*
[2]*Department of Physics, Faculty of Mathematics and Natural Sciences, University of Mataram, Mataram, 83125, West Nusa Tenggara, Indonesia*
[3]*Department of Physics, Faculty of Mathematics and Natural Sciences, Universitas Brawijaya, Malang, 65145, East Java, Indonesia*
[4]*Department of Animal Sciences, Faculty of Animal Sciences, University of Mataram, Mataram, 83125, West Nusa Tenggara, Indonesia*

Received: 26 September 2025/Accepted: 29 June 2026

ABSTRACT

The valorization of *Pinctada maxima* shell waste as a calcium source offers a sustainable route for developing calcium phosphate bioceramics. This study evaluated the effect of post-synthesis calcination duration on the physicochemical properties of hydroxyapatite/β-tricalcium phosphate (HAp/β-TCP) powders derived from *Pinctada maxima* shells. Shell-derived CaO was used as the calcium precursor, followed by wet precipitation to obtain calcium phosphate precursors and post-synthesis calcination at 700 °C for 3, 6, 9, and 12 h. The resulting powders were characterized using EDX, proximate analysis, FTIR, XRD, PSA, and SEM. The Ca/P ratios varied with calcination duration, with values of 1.70, 1.61, 1.54, and 1.53 for Samples A, B, C, and D, respectively. Proximate analysis showed high inorganic purity, indicated by low moisture content (0.01-0.08%), high ash content (99.93-99.99%), and negligible fat residues (0.0236-0.0457%). FTIR confirmed the presence of PO_4^{3-} and OH^- functional groups, while XRD qualitatively confirmed the coexistence of HAp and β-TCP phases. Among the tested conditions, the 9 h calcination treatment (Sample C) showed the most promising overall physicochemical profile, with a Ca/P ratio of 1.54, distinct HAp/β-TCP diffraction features, favourable crystallographic parameters, and a coherent particle size distribution (mean = 96.61 μm; D50 = 101.10 μm). SEM observations supported the PSA results, showing granular aggregates and irregular agglomerates typical of wet-synthesized calcium phosphate powders. However, quantitative HAp:β-TCP phase fractions were not determined; therefore, Rietveld refinement or the RIR method is required to confirm phase optimization. Overall, *Pinctada maxima* shell waste shows potential as a sustainable precursor for HAp/β-TCP powder development, although biological, mechanical, and benchmark evaluations are still needed before clinical applicability can be established.

Keywords: Biphasic calcium phosphate; calcination duration; HAp/β-TCP; marine-derived biomaterial; particle agglomeration; *Pinctada maxima* shell

ABSTRAK

Valorisasi sisa cangkerang *Pinctada maxima* sebagai sumber kalsium menawarkan pendekatan mampan untuk membangunkan bioseramik kalsium fosfat. Kajian ini menilai kesan tempoh pengkalsinan pascasintesis terhadap sifat fizikokimia serbuk hidroksiapatit/β-trikalsium fosfat (HAp/β-TCP) yang diperoleh daripada cangkerang *Pinctada maxima*. CaO terbitan cangkerang digunakan sebagai prekursor kalsium, diikuti kaedah pemendakan basah untuk menghasilkan prekursor kalsium fosfat dan pengkalsinan pascasintesis pada suhu 700 °C selama 3, 6, 9 dan 12 jam. Serbuk yang terhasil dicirikan menggunakan EDX, analisis proksimat, FTIR, XRD, PSA dan SEM. Nisbah Ca/P berubah mengikut tempoh pengkalsinan dengan nilai 1.70, 1.61, 1.54 dan 1.53 masing-masing bagi sampel A, B, C dan D. Analisis proksimat menunjukkan ketulenan tak organik yang tinggi, ditunjukkan oleh kandungan lembapan yang rendah (0.01-0.08%), kandungan abu yang tinggi (99.93-99.99%) dan sisa lemak yang boleh diabaikan (0.0236-0.0457%). FTIR mengesahkan kehadiran kumpulan berfungsi PO_4^{3-} dan OH^-, manakala XRD secara kualitatif

mengesahkan kewujudan bersama fasa HAp dan β-TCP. Antara keadaan yang diuji, rawatan pengkalsinan selama 9 jam (Sampel C) menunjukkan profil fizikokimia keseluruhan yang paling berpotensi dengan nisbah Ca/P 1.54, ciri pembelauan HAp/β-TCP yang jelas, parameter kristalografi yang baik dan taburan saiz zarah yang koheren (min = 96.61 μm; D50 = 101.10 μm). Pemerhatian SEM menyokong keputusan PSA dengan menunjukkan agregat bergranul dan aglomerat tidak sekata yang lazim bagi serbuk kalsium fosfat yang disintesis melalui kaedah basah. Walau bagaimanapun, pecahan kuantitatif fasa HAp:β-TCP belum ditentukan; oleh itu, penapisan Rietveld atau kaedah RIR diperlukan untuk mengesahkan pengoptimuman fasa. Secara keseluruhan, sisa cangkerang *Pinctada maxima* menunjukkan potensi sebagai prekursor mampan untuk pembangunan serbuk HAp/β-TCP, namun penilaian biologi, mekanikal dan perbandingan dengan bahan penanda aras masih diperlukan sebelum kebolehgunaan klinikal dapat dipastikan.

Kata kunci: Aglomerasi zarah; biobahan terbitan marin; cangkerang *Pinctada maxima*; HAp/β-TCP; kalsium fosfat dwifasa; tempoh kalsinasi

INTRODUCTION

Bone tissue engineering continues to require biomaterials that can support bone repair after trauma, degenerative disease, tumour resection or surgical intervention. Calcium phosphate bioceramics are widely investigated for this purpose because their composition resembles the mineral phase of bone. Hydroxyapatite (HAp) provides chemical stability and osteoconductive potential, whereas β-tricalcium phosphate (β-TCP) is more soluble and can contribute to material resorption. A biphasic calcium phosphate (BCP) system that combines HAp and β-TCP can therefore provide a tunable balance between structural persistence and degradability (Ebrahimi, Botelho & Dorozhkin 2017; LeGeros et al. 2003; Skliarenko et al. 2024). Marine-derived biominerals are attractive calcium sources for producing calcium phosphate ceramics. Mollusc shells, like oyster cockle and pearl shells are for the most part built from calcium carbonate, and they can be transformed into calcium oxide then, into calcium phosphate phases. Earlier works suggest that shell-derived precursors are able to make HAp or HAp/β-TCP powders, with properties that look useful for biomedical materials (Muntean et al. 2024; Mustaffa, Mohd Yusof & Abdullah 2015; Wu et al. 2017). This approach also supports circular-bioeconomy principles by converting aquaculture by-products into higher-value functional materials.

Even with this possible outlook, the physicochemical traits of shell derived calcium phosphate powders, still remain a bit on the sensitive side to how the synthesis is done. The calcination temperature, along with how long it is held there, tends to shape precursor decomposition and also affects phase transformation, crystallite growth, and even particle clustering. For BCP materials, the HAp:β-TCP phase ratio is particularly important because the two phases have different stability and dissolution behaviour (Chu et al. 2013; Farzadi et al. 2011). Therefore, time-dependent thermal processing requires careful characterization rather than relying only on qualitative phase identification. Most previous studies on natural-source calcium phosphate have emphasized calcination temperature, whereas the effect of post-synthesis calcination duration on *Pinctada maxima*-derived HAp/β-TCP remains less clearly described. In addition, many studies report phase presence from XRD without directly quantifying the HAp and β-TCP fractions. Because qualitative XRD cannot determine the actual biphasic ratio, quantitative phase analysis using Rietveld refinement or the reference intensity ratio method is needed when the research objective is to optimize HAp:β-TCP composition (Döbelin 2015).

The present study evaluates the physicochemical characteristics of HAp/β-TCP powders synthesized from *Pinctada maxima* shell waste and compares the effects of post-synthesis calcination at 700 °C for 3, 6, 9, and 12 h. The characterization workflow included EDX, proximate analysis, FTIR, XRD, and PSA to assess elemental composition, Ca/P ratio, functional groups, crystallographic parameters, and particle-size distribution. The working hypothesis was that increasing post-synthesis calcination duration would modify the Ca/P ratio, functional-group expression, crystallite development, and particle-size distribution of shell-derived calcium phosphate powders. Within the limits of the data that is available, the study points out the calcination condition that shows the most favourable physicochemical profile, and gives a base for later quantitative phase refinement, morphological checking, and biological validation. It is not exactly exhaustive, but it is enough to proceed.

MATERIALS AND METHODS

In this study, calcium oxide (CaO) that comes from calcined pearl oyster shell waste (*Pinctada maxima*) was used as the main starter raw material to synthesize hydroxyapatite/beta-tricalcium phosphate (HAp/β-TCP). Analytical-grade chemicals were distilled water, hydrochloric acid (HCl 37% Merck, Germany), phosphoric acid (H_3PO_4 85% Merck, Germany), Whatman filter paper (Grade 42, 2.5 μm GE Healthcare UK), and universal pH sticks from Macherey-Nagel, Germany. The preparation involved washing, drying (70 °C, 2 h), grinding, milling, and calcination of the shells at 900 °C for 6 h

to obtain CaO, following Rahayu, Kurniawidi and Gani (2018). A 0.5 M calcium hydroxide [$Ca(OH)_2$] solution was prepared from CaO and reacted with H_3PO_4 by wet precipitation, with pH maintained at ~5 using HCl (Figure 1). This pH was deliberately selected, as precipitation under mildly acidic conditions (pH ~5) favours the co-formation of HAp and β-TCP phases, whereas alkaline conditions (pH ~9–11) tend to promote a predominantly HAp-rich product (Tran et al. 2025). At pH ~5, the wet precipitation step was intended to form a calcium phosphate precursor rather than phase-pure HAp. The subsequent calcination step promoted the crystallization and transformation of this precursor into HAp/β-TCP phases, as confirmed by XRD and FTIR. The suspension was homogenized at 80 °C for 1 h, then aged for 24 h at room temperature to promote precipitation. The resulting precipitate was filtered, dried (100 °C), ground, and recalcined at 700 °C for 3, 6, 9, and 12 h. The powders were cooled, reground, and stored in airtight containers. Variation in calcination duration was designed to evaluate its effect on phase formation, Ca/P ratio, crystallinity, and particle size of the synthesized HAp/β-TCP. The initial calcination at 900 °C for 6 h was applied only to convert the shell-derived $CaCO_3$ into CaO precursor. The subsequent calcination at 700 °C for 3-12 h was applied to the synthesized calcium phosphate powder. Therefore, the reported calcination duration refers specifically to the post-synthesis thermal treatment, not to the total thermal exposure of the original shell precursor.

From preparation to calcination, four types of powders were produced: Sample A (700 °C, 3 h), Sample B (700 °C, 6 h), Sample C (700 °C, 9 h), and Sample D (700 °C, 12 h), which were then subjected to comprehensive physicochemical characterisation, including Energy Dispersive X-ray Spectroscopy (EDX), proximate analysis, Fourier Transform Infrared Spectroscopy (FTIR), X-ray Diffraction (XRD), and Particle Size Analysis (PSA). EDX spectroscopy was basically used to find the elemental composition and the Ca/P ratio. The measurements were done after the samples were sputter coated with gold, just to reduce the charging effects or whatever. For the Ca/P ratio, the calculation was made from the atomic percentages of Ca and P that came out of the spectra, and then compared with the optimal interval of 1.50-1.67 which is typically needed for biphasic hydroxyapatite and β-tricalcium phosphate biomaterials.

Proximate analysis was done to get a view of the moisture, ash, and fat levels, using standard protocols that we adjusted a bit for powder samples. For moisture, we followed SNI 2354.2:2006 but with some change for powders, then the ash value was obtained by burning the sample in a muffle furnace 600 °C for about 6 h. For the fat content, we used a gravimetric extraction method with hexane, after that HCl digestion was performed first. Proximate analyses were performed as single measurements for each sample, and the results are reported as individual values without statistical analysis. The findings were assessed against biomedical powder benchmarks, where the moisture content has to stay under 0.1%, the ash level needs to go past 99% and the fat remains should be basically negligible, so biocompatibility is maintained and the chance of inflammatory response risk stays minimal.

FTIR Spectroscopy was done via KBr pellet procedures, and the spectra were taken in the range about 500−4000 cm^{-1}. We saw signal peaks that match phosphate (PO_4^{3-}), hydroxyl (OH^-), plus carbonate (CO_3^{2-}) related groups, and we treated them like usual functional group signs for calcium phosphate bioceramic materials. Basically, those markers are pretty standard for this kind of calcium phosphate bioceramics. XRD analysis was conducted using a PANalytical X'Pert PRO diffractometer with CuKα radiation (λ = 1.5406 Å) in the 2θ range of 10–60° at 0.02° step size. Phase identification was performed with JCPDS references for HAp and β-TCP. Peaks were compared with JCPDS references for HAp (09-0432) and β-TCP (09-0169). The main diffraction peaks selected for crystallographic interpretation were the HAp reflections around 2θ ≈ 31.8–32.4° and the β-TCP reflections around 2θ ≈ 28.7–31.0°, based on their intensity and correspondence with the reference patterns.

Crystallite size was estimated using the Scherrer equation:

$$D = \frac{K\lambda}{\beta \cos \theta}$$

where D is the crystallite size; K is the shape factor, assumed to be 0.9; λ is the X-ray wavelength; β is the full width at half maximum (FWHM) of the selected diffraction peak in radians, and θ is the Bragg angle. Crystallinity was estimated from the relative area of crystalline peaks to the total diffracted area using the following equation:

$$X_C\,(\%) = \frac{A_C}{A_C + A_a}\, x\ 100$$

where X_c is the crystallinity percentage; A_c is the integrated area of crystalline diffraction peak; and *Aa* is the area of amorphous background. Background subtraction and peak fitting were performed prior to crystallinity estimation to minimize the contribution of baseline noise and peak overlap. The crystallographic parameters, including FWHM, lattice parameters, crystallite size, microstrain, dislocation density, and crystallinity, were interpreted together to avoid over-reliance on a single crystallinity value. Quantitative HAp:β-TCP phase fractions were not determined

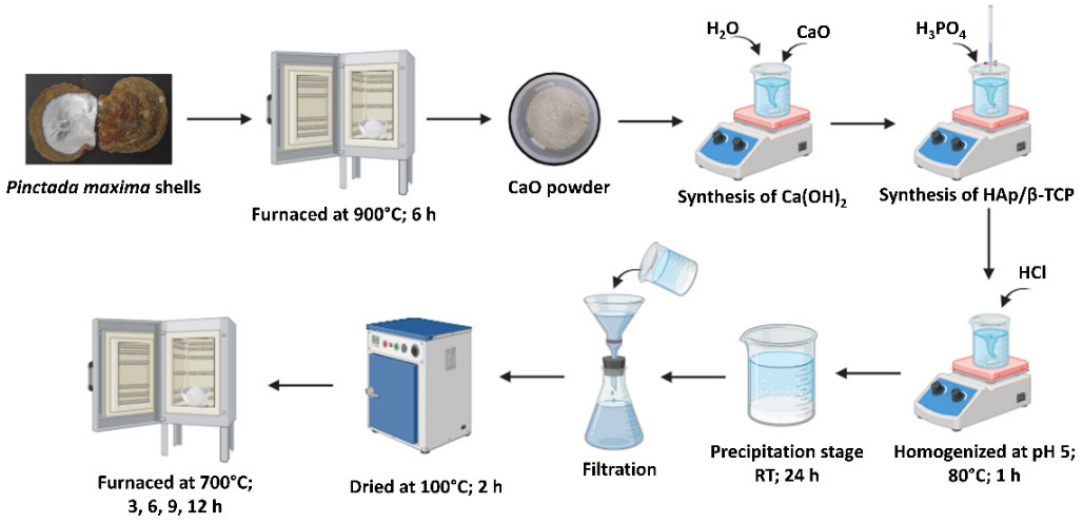

FIGURE 1. Schematic illustration of HAp/β-TCP synthesis using precipitation and calcination treatments

from the available dataset. Therefore, the presence of HAp and β-TCP was confirmed qualitatively based on peak matching with JCPDS references.

The morphology of the synthesized HAp/β-TCP powders was observed using scanning electron microscopy (SEM). Powder samples were mounted on aluminium stubs with double-sided carbon tape and sputter-coated with gold to improve conductivity. SEM observations were performed under high-vacuum conditions at an accelerating voltage 15 kV. Images were collected at selected magnifications to evaluate particle morphology, surface texture, and agglomeration behaviour of samples calcined at 700 °C for 3, 6, 9, and 12 h. The SEM findings were correlated with PSA data to assess whether the measured micrometre-scale particle sizes were associated with particle agglomeration. Particle Size Analysis (PSA) was carried out using a laser diffraction method (Malvern Mastersizer 2000, UK). Approximately 0.1 g of each powder was dispersed in ethanol, ultrasonicatedfor 15 min, and analysed for mean particle size (D50). The size distributions were analysed based on clinical requirements for bone substitute powders, which typically range between 50 and 150 µm for adequate porosity and osteointegration.

RESULTS AND DISCUSSION

This section shows the synthesis and characterization of HAp/β-TCP that was gotten from *Pinctada maxima* shells after the calcination step at 3, 6, 9, and 12 h. The work focuses on how calcination time messes with the physicochemical behavior of the powders, like their elemental makeup and the Ca/P ratio (EDX) plus the proximate composition. Also included is the detection of functional group signatures through FTIR, then the crystalline phases and the crystallinity via XRD, and finally the particle size distribution. In a way each characterization route offers extra viewpoints about phase transformation, the steadiness of the structure, and the overall morphology, and those are then looked at alongside their relevance as prospects for resorbable bone matrices. The EDX spectra for the four synthesized samples, each treated with a different calcination duration, pointed to noticeably different elemental profiles (Figure 2). Strong calcium (Ca) and phosphorus (P) peaks were clearly seen, and this supports the idea that calcium phosphate phases were formed, while oxygen (O) stayed as the dominant component throughout. Beyond that, smaller amounts of trace elements such as Mg, Na, Al, Si, Zn, and Fe showed up, they were only minor but still present, and they are most likely coming from precursor impurities or from a sort of incidental uptake during the synthesis process.

Quantitative analysis showed some distinct variations in the Ca/P atomic ratios depending on calcination time (Table 1). Sample A has the biggest Ca/P ratio at 1.70, just a bit over the expected stoichiometric hydroxyapatite value (1.67). This sort of Ca-rich makeup could come from an incomplete conversion where CaO does not fully turn into the phosphate phases. Sample B, on the other hand, gives Ca/P = 1.61 which is still inside the usual 1.50-1.67 span reported for biphasic calcium phosphate. That outcome implies a balanced coexistence of HAp and β-TCP. Samples C (1.54) and D (1.53) end up lower, and they sit close to the β-TCP side, so there is likely an increasing presence of Ca-deficient phases, which in turn tends to favour higher resorbability.

Ca/P atomic ratio analysis at various calcination times provides important insights into the composition and functionality of calcium phosphate. Sample A had the highest Ca/P ratio of 1.70 (larger than HAp's

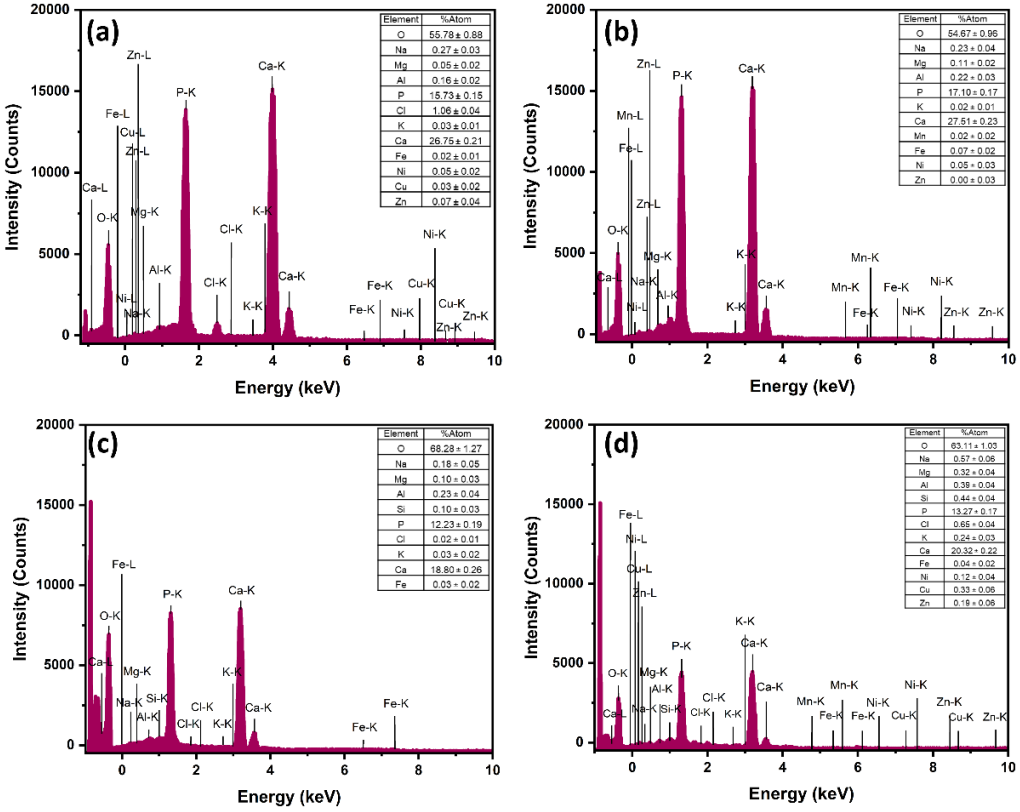

FIGURE 2. EDX spectra of HAp/β-TCP (a) 3 h, (b) 6 h, (c) 9 h, and (d) 12 h

stoichiometric of 1.67), indicating a Ca-rich composition, most likely due to insufficient conversion of CaO into phosphate phases, as calcination parameters have been shown to have a substantial influence on phase formation (Italiano et al. 2024; Putkham, Ladhan & Putkham 2020). In contrast, Sample B showed a Ca/P ratio of 1.61, which is within the 1.50-1.67 range for biphasic calcium phosphate (BCP). This proposes a balanced combination of HAp and β-TCP, which increases its applicability by integrating mechanical stability and β-TCP's resorbability (Italiano et al. 2024). Samples C and D showed decreased Ca/P ratios of 1.54 and 1.53, similar to the β-TCP domain. This suggests a Ca-deficient phase, which has been shown to increase bioactivity and tissue integration (Firdaus, Wahfiudin & Aprilianti 2022; Yanti & Resmalina 2021). Notably, Ca/P ratio of Sample C is close to the standard reference value of 1.55 for biphasic HAp/β-TCP ceramics, making it suitable for resorbable bone matrix applications (Duta, Dorcioman & Grumezescu 2021).

Biomedical experts usually suggest Ca/P ratios around 1.50-1.67 for resorbable bone substitutes, mostly because it helps keep the scaffold's structural integrity while also letting it degrade in a more controlled way (Dinatha et al. 2023). Sample A had pretty significant amounts of calcium, which may limit bio-resorption, while Sample B showed a balanced biphasic profile overall. Sample D suggested a shift toward β-TCP dominance, which could possibly lower long-term stability a bit. In a more striking way, Sample C looks like the optimal option, because it lines up closely with the targeted Ca/P ratio, and it also shows its distinctive qualities as a resorbable bone matrix candidate that comes from *Pinctada maxima* shells. Altogether, these results point out how calcination time is critically relevant for modifying physicochemical properties, and they also underline the opportunity of sustainable marine-derived precursors for biomedical uses (Kristianto, Sari & Yusuf 2022; Putkham, Ladhan & Putkham 2020).

The proximate analysis suggests high inorganic content and low organic residues, and that lines up with what EDX analysis shows (Figure 2). Table 2 also demonstrates consistently low moisture content, around 0.01-0.08 %, so the volatile components got eliminated properly because calcination temperatures were pretty high (Mohd Pu'ad et al. 2020). Sample D (12 h) showed a slightly higher moisture value (0.08%), most likely due to ambient moisture uptake during cooling and storage rather than incomplete volatile removal, as its ash content (99.94%) remained among the highest of the four samples (Espanol et al. 2023). This unexpected outcome might indicate post-calcination moisture reabsorption happening while cooling, handling or storage, since calcium phosphate powders can take up water from the surrounding air. In the same way the ash level which sits around 99.93% to 99.99% points to the stronger

TABLE 1. Ca/P ratio of HAp/β-TCP

Sample	%Atom		Ca/P ratio
	Ca	P	
A	26.75	15.73	1.70
B	27.51	17.10	1.61
C	18.80	12.23	1.54
D	20.32	13.27	1.53

TABLE 2. Proximate analysis of each HAp/β-TCP sample

Sample	Moisture content (%)	Ash content (%)	Fat content (%)
A	0.02	99.93	0.0457
B	0.04	99.97	0.0390
C	0.01	99.99	0.0329
D	0.08	99.94	0.0236

presence of mineral phases, it also helps confirm the purity of the synthesised powders (Ahmad & Elkilania 2022). The low fat (0.0236-0.0457%), indicates that the residual organic compounds were effectively removed during calcination, so the inorganic matrix stayed highly purified. Prior works have shown that getting rid of fats and other organic leftovers is essential for reaching hydroxyapatite with better crystallinity, structural endurance, and repeatable outcomes for medical use (Firdaus, Wahfiudin & Aprilianti 2022). When the organic contamination is reduced, it also lowers the chances of uninvited biological responses, and it supports the making of bioceramics with more consistent physicochemical behavior (Ishtiaque et al. 2022; Wang, Zhao & Wang 2021). Between the four samples, Sample C showed the lowest moisture level at 0.01%, the greatest ash amount 99.99%, and also the thinnest fat fraction 0.0329%. Those traits then aligned with its Ca/P ratio, so it looks like a promising option for resorbable bone matrix uses. Also, the ability of EDX to map elemental distribution in calcium phosphates was pretty convincingly shown, making sure that the stoichiometry and the overall purity are kept on track during bioceramic synthesis (Weinand et al. 2022). Since the proximate analyses were basically done as one single measurement, there was not any proper statistical comparison, between the samples could not really be carried out. So, those differences that we saw really should be treated as descriptive trends, rather than as statistically confirmed differences. In general, our results point out that Sample C shows its originality and also looks appropriate for use in bone regeneration techniques.

In the FTIR spectra, it was possible to notice the presence of functional groups related to the calcium phosphate phases (Figure 3). The absorption bands from phosphate (PO_4^(3-)) appeared roughly between 1090, 960, and 600 cm^{-1}, and this behavior confirms the formation of HAp together with β-TCP type structures. In particular, samples B and C had a strong OH^- stretching vibration around 3570 cm^{-1}, which points toward a successful embedding of hydroxyl groups into the apatite lattice. Carbonate (CO_3^{2-}) substitution bands at 1450 and 875 cm^{-1} show partial replacement of phosphate ions, enhancing bioactivity in bone-related applications.

Sample A, with a higher Ca/P ratio of 1.70, showed weaker OH^- and PO_4^{3-} absorption bands, indicating incomplete phase conversion and surplus calcium (Ardiansyah, Saraswaty & Risdian 2023). In contrast, Sample B had balanced absorption intensities, indicating a steady coexistence of HAp and β-TCP. This is important for improving bioactivity and mechanical performance in phosphate-based biomaterials (Ebrahimi, Botelho & Dorozhkin 2017). Sample C had the most prominent phosphate and hydroxyl bands and few carbonate traces, which corresponded to its optimal Ca/P ratio and excellent proximate composition, establishing its structural purity and stability, as highlighted in recent studies (Ftiti et al. 2024). Sample D showed comparable absorption characteristics, but with significantly lower band sharpness. This suggests possible over-resorption of phases due to prolonged calcination, which may influence long-term stability in biomineral structures (Valadão Cardoso & Novaes Ferreira 2024). Overall, these FTIR spectra show that Sample C has excellent structural properties, validating its place as the most suitable candidate for resorbable bone matrix applications.

The XRD spectra of HAp/β-TCP powders showed separate peaks for HAp and β-TCP, suggesting the

formation of biphasic calcium phosphate (Figure 4). These findings match the FTIR data, demonstrating the structural integrity of the synthesized powders.

The XRD results show that post- synthesis calcination duration had a clear impact on how wide the peaks are, their intensity, and also on the crystallographic parameters. It also matters that every sample went through the exact same first calcination step, basically to get the CaO precursor ready. So, the differences seen from Samples A to D are mostly coming from the changes in the post-synthesis calcination duration, not from any differences in the earlier thermal treatment. The earlier idea about Sample A being 'poorly crystalline' was revisited, because Table 3 indicates that Sample A actually has the highest overall crystallinity value (79.67%). A more consistent way to read it is that Sample A does have a high calculated crystallinity percentage, but it also shows a broad HAp peak, a smaller HAp crystallite size, and higher microstrain. In other words, the HAp crystallites may be less ordered or less stable during development. Samples B through D, on the other hand, show narrower peaks and larger crystallite sizes, which points to better crystallite growth when the post-synthesis calcination time is longer. Sample C gives a good combination in terms of Ca/P ratio, FTIR signatures and crystallographic parameters but the real HAp:β-TCP ratio still needs to be quantified. Although XRD confirmed the coexistence of HAp and β-TCP phases, the actual HAp:β-TCP weight fractions could not be determined from the available dataset. Therefore, Sample C is not interpreted as having the quantitatively best biphasic composition, but rather as the sample with the most promising overall physicochemical profile based on its Ca/P ratio, diffraction peak sharpness, functional group stability, inorganic purity, and particle size distribution.

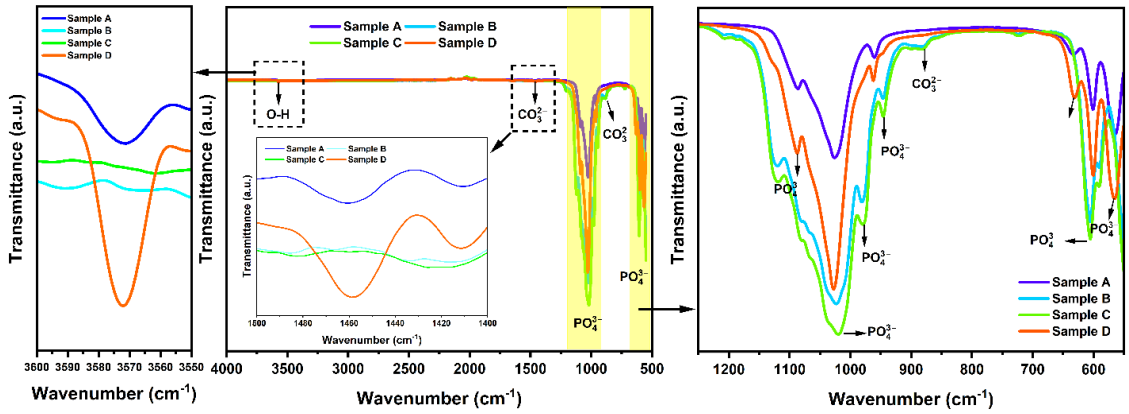

FIGURE 3. FTIR Spectra of HAp/β-TCP

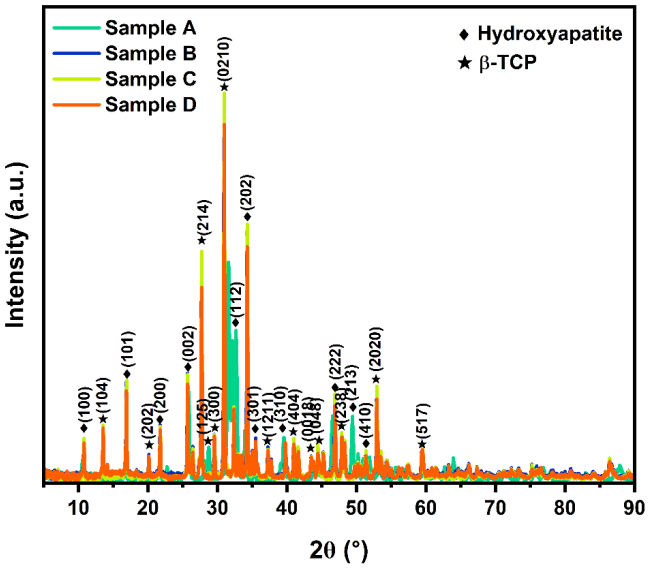

FIGURE 4. XRD spectra of HAp/β-TCP

The crystallographic parameters (Table 3) show that Sample A had the largest HAp FWHM (1.44°), the smallest HAp crystallite size (5.72 nm), and the highest microstrain (21.97 × 10^{-3}), indicating greater lattice distortion and smaller coherent crystalline domains despite its high calculated crystallinity value, indicating incomplete crystallization and structural instability, consistent with the relationship between FWHM, crystallite size, and poor crystallinity (Borštnar, Lengauer & Dolenec 2021; Minh 2021). Samples B–D had narrower FWHM values (~0.16–0.17°), larger crystallite sizes (~49–52 nm), lower microstrain (~2.4–2.6 × 10^{-3}), and lower dislocation density (~3.8–4.1 × 10^{-4} nm^{-2}). These results suggest that prolonged post-synthesis calcination enhanced crystallite development and microstructural ordering, in line with reports that extended calcination enhances crystalline development in ceramic compounds (Widyastuti & Yusuf 2024). Among them, Sample C (9 h) achieved the most favourable balance, with a crystallite size of 49.56 nm, microstrain of 2.51 × 10^{-3}, and dislocation density of 4.1 × 10^{-4} nm^{-2}, representing an optimal compromise between stability and defect minimization. Crystallinity values stayed pretty high in all the samples, around 69.01-79.67%, and Sample C showed the most favourable overall profile, it had purity, stability and structural integrity, all together. So, this basically confirms that 9 h of calcination gives the best condition for making HAp/β-TCP powders, which are suitable for use as resorbable bone matrix materials (Fujioka-Kobayashi et al. 2022; Lang et al. 2025; Moreira Filho, Wykrota & Lobo 2021; Saulacic et al. 2021).

Figure 5 shows the particle size distribution of HAp/β-TCP under different calcination durations, and this gives important correlations with the structural features that are described through EDX, FTIR, and XRD. Sample A had the smallest average particle size (75.09 μm, D50 = 65.61 μm), which seems to match its broader XRD peaks, weaker FTIR absorptions, and a higher Ca/P ratio. That overall suggests a rather incomplete phase development, reduced crystallinity and a microstructure that is less stable than others (Carvalho et al. 2022; Liu et al. 2021). In contrast, Sample B demonstrated a larger mean size (87.67 μm, D50 = 90.69 μm), which reflected improved crystallinity and phase balance as related to XRD and FTIR analyses, alongside its Ca/P ratio, suggesting favourable biphasic coexistence. Prolonged calcination in Sample C yielded the coarsest distribution (mean = 96.61 μm, D50 = 101.10 μm), which corresponded with the sharpest XRD peaks and most distinct FTIR phosphate and hydroxyl bands, indicating pronounced crystallinity and structural stability of the biphasic material (Shigemitsu et al. 2022). Such crystallinity is often linked to enhanced mechanical behavior and greater biological activity, even if too much particle growth might lower the uniformity a bit. At the same time, Sample D showed a reduction in size mean = 81.88 μm, D50 = 69.82 μm which could be caused by fragmentation or by some stabilization action during long calcination periods. This lines up with the broadening of the β-TCP reflections in XRD and also with the drop in the Ca/P ratio (1.53) as was reported before when people described morphological shifts after extended thermal treatment (Ningsih et al. 2021).

The micrometre-scale PSA results should not be directly compared with the nanometre-scale crystallite sizes from XRD as if both measured the same feature. XRD-derived crystallite size represents coherent crystalline domains, whereas PSA measures particle or agglomerate size in dispersion. The approximately thousand-fold difference therefore suggests that the powders consisted of agglomerates of nanoscale crystallites formed during drying, calcination, grinding or storage. SEM imaging would be useful to verify this agglomeration and to evaluate particle morphology (Figure 6). Taken together, the EDX, FTIR, XRD, and PSA results support Sample C as the most promising physicochemical condition in this dataset, but not yet as a quantitatively confirmed optimum HAp:β-TCP composition.

Figure 6 shows the morphology of HAp/β-TCP synthesized at 700 °C with calcination times of 3, 6, 9, and 12 h. All samples exhibited a morphology consisting of fine particle aggregates that formed granular structures and irregular agglomerates, which is a common characteristic of BCP produced by the wet synthesis method due to the high surface energy of the primary particles, which promotes agglomeration during calcination. Similar results were reported by Carvalho et al. (2022) who observed the formation of particle agglomerates with irregular shapes in HAp/β-TCP after heat treatment. Sample A exhibited agglomerates with a heterogeneous distribution and relatively large interparticle spaces, indicating still-limited crystal growth and interparticle diffusion; this is consistent with the PSA results showing the smallest average particle size. Sample B exhibited a more homogeneous and dense structure, as increased thermal energy promoted surface diffusion and stronger intergranular bonding, as evidenced by the increase to 87.67 μm. Satish et al. (2023) reported that increased heat treatment of BCP led to grain growth and structural densification, which contributed to improved microstructural quality. The most significant morphological changes were observed in Sample C, with particle agglomerates appearing larger, more homogeneous, and densely packed with relatively uniform primary particles. The material's surface appeared more compact than that of the other samples, indicating that the processes of diffusion and crystal growth occurred effectively. These SEM results correlate with the PSA results showing the largest average particle size, indicating that a 9-h calcination time provides optimal thermal energy for crystal growth and microstructural reorganization. Sample D (12 h) exhibits a more compact morphology but with smaller agglomerate sizes compared to Sample C, indicating

TABLE 3. Crystalllographic of HAp/β-TCP

Parameter	Sample A		Sample B		Sample C		Sample D	
	HAp	β-TCP	HAp	β-TCP	HAp	β-TCP	HAp	β-TCP
2θ (°)	31.99	28.73	32.37	30.96	32.39	30.97	32.38	30.97
Lattice ($a = b$; c)	9.48; 6.88	10.43; 37.37	9.40; 6.88	10.41; 37.34	9.42; 6.88	10.40; 37.36	9.40; 6.90	10.42; 37.41
FWHM (°)	1.44	0.33	0.16	0.16	0.17	0.16	0.17	0.17
d_{hkl} (Å)	2.80	3.11	2.76	2.89	2.76	2.88	2.76	2.88
D (nm)	5.72	25.14	51.59	50.19	49.56	50.73	49.36	49.91
ε ($\times 10^{-3}$)	21.97	5.56	2.41	2.59	2.51	2.56	2.52	2.60
δ ($\times 10^{-4}$ nm^{-2})	305.2	15.8	3.8	4.0	4.1	3.9	4.1	4.0
Crystallinity (%)	79.67		74.52		75.59		69.01	
Structure	Hxg*	Rbh*	Hxg	Rbh	Hxg	Rbh	Hxg	Rbh

Hxg*= Hexagonal; Rbh*= Rhombohedral

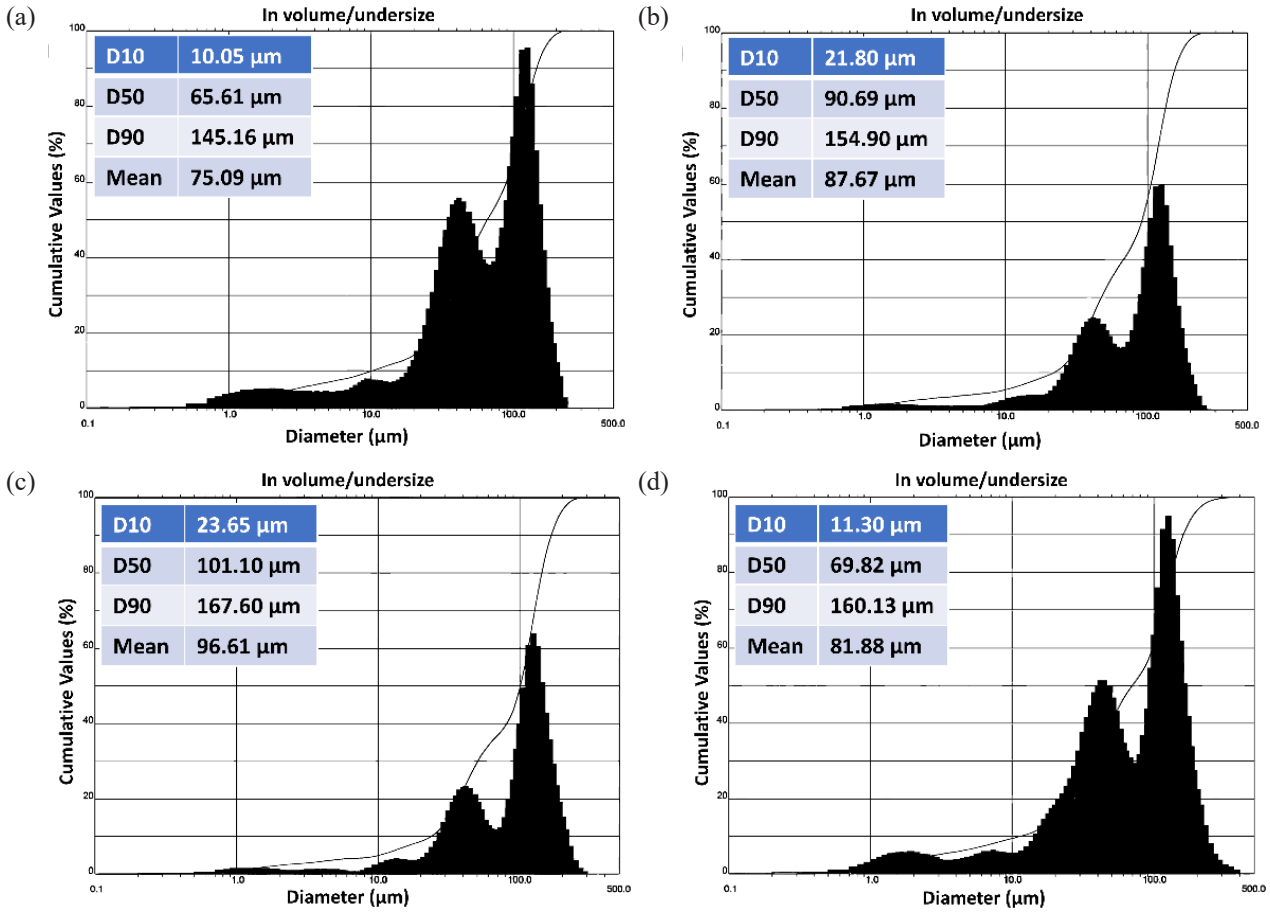

FIGURE 5. Particle size distribution of HAp/β-TCP (a) 3 h, (b) 6 h, (c) 9 h, and (d) 12 h

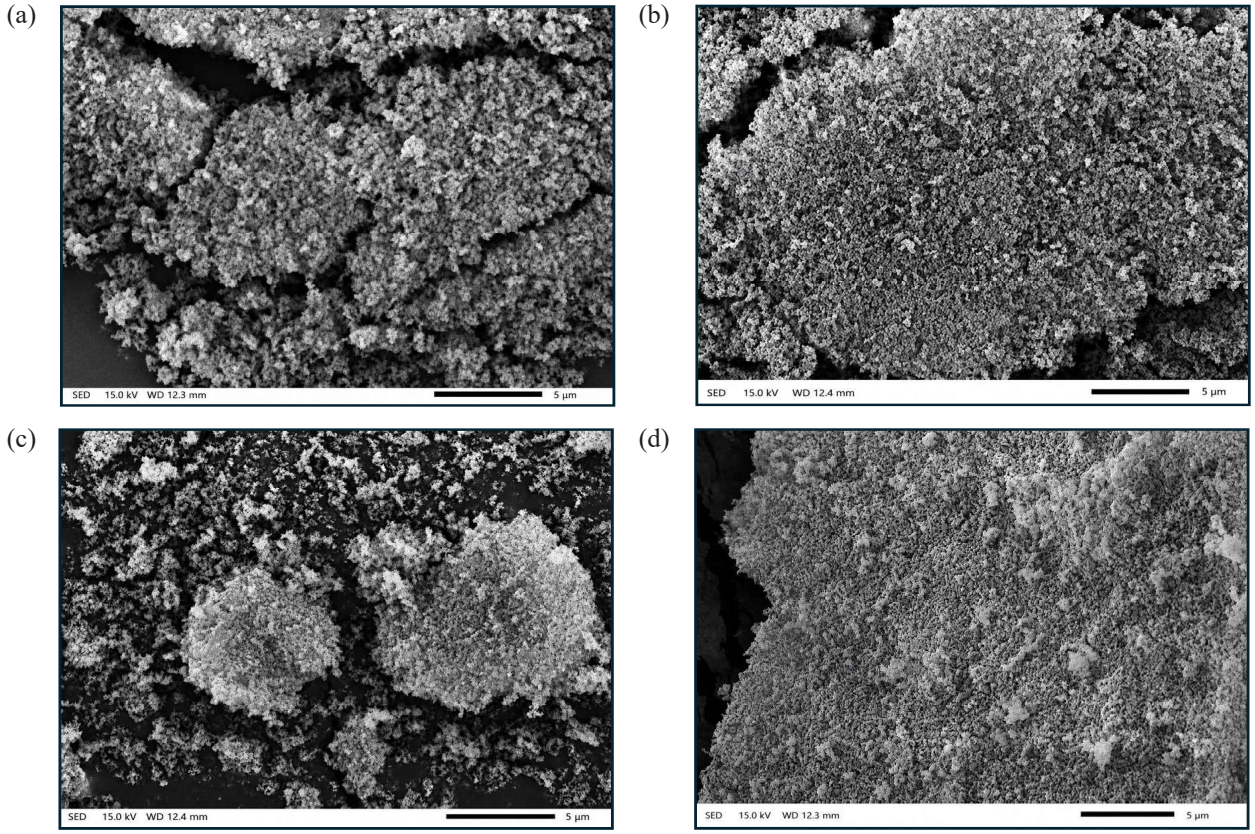

FIGURE 6. Morphology of HAp/β-TCP (a) 3 h, (b) 6 h, (c) 9 h, and (d) 12 h

partial fragmentation and microstructural reorganization due to phase equilibrium changes during prolonged calcination (Feng et al. 2021). Overall, Sample C exhibited the best balance between morphological homogeneity and particle growth, making a calcination time of 9 h at 700 °C the optimal condition for producing BCP with stable microstructural characteristics that have the potential to support bioactivity and mechanical properties for bone regeneration applications.

In conclusion, this study managed to show that *Pinctada maxima* shell waste can be turned into a new calcium source for making hydroxyapatite/β-tricalcium phosphate (HAp/β-TCP) bioceramics, but only when the calcination is carefully controlled. The full characterization was done with EDX, proximate analysis, FTIR, XRD, and PSA, and it basically verified that the calcination time really matters, it changes phase composition, crystallinity levels, and also the particle size distribution. Overall, out of all the treatments, Sample C (700 °C, 9 h) gave the best overall results. It had a favourable Ca/P ratio of 1.54 which is pretty close to the biphasic reference value 1.55. It also showed sharp, intense diffraction peaks, which suggests high crystallinity. Meanwhile in FTIR, there were strong absorptions linked to phosphate and hydroxyl groups, and the particle size distribution looked well balanced, so it should fit biomedical needs. So these results suggest that Sample C is the best compromise between HAp stability and β-TCP resorbability, which is appropriate for the intended application for resorbable bone matrices. Also, the novelty here is that, as far as we know, this work was the first time *Pinctada maxima* shell waste was used as a precursor to produce high-purity HAp/β-TCP, with physicochemical properties that are tailored on purpose. That means it supports scientific progress in biomaterials research while also promoting a more sustainable way to use marine biowaste for regenerative medicine applications. To avoid interpreting the present findings in isolation, Sample C was compared with previously reported HAp/β-TCP materials derived from synthetic and biogenic calcium sources. Its Ca/P ratio of 1.54 falls within the range commonly associated with calcium-deficient or β-TCP-containing biphasic calcium phosphate systems, while its micrometre-scale particle size distribution is comparable to powder forms reported for bone substitute development. However, because no commercial benchmark material was tested directly in this study and no biological evaluation was performed, Sample C should be considered a promising physicochemical candidate rather than a clinically validated bone substitute.

CONCLUSIONS

This study demonstrates that post-synthesis calcination duration at 700 °C plays an important role in regulating the physicochemical properties of hydroxyapatite/β-tricalcium phosphate (HAp/β-TCP) powders derived from *Pinctada maxima* shell waste. The variation in calcination time affected the Ca/P ratio, crystallographic parameters, functional group stability, particle aggregation, and overall powder characteristics. The Ca/P ratios changed from 1.70 in Sample A to 1.61, 1.54, and 1.53 in Samples B, C, and D, respectively, indicating that longer post-synthesis calcination influenced the calcium phosphate composition of the powders. Proximate analysis further showed low moisture content, high ash content, and negligible fat residues, confirming the high inorganic purity of the synthesized materials.

Among the tested conditions, Sample C, obtained after 9 h of post-synthesis calcination, showed the most promising overall physicochemical profile. This sample showed a Ca/P ratio around 1.54, with clear HAp/β-TCP diffraction sort of features, plus stable PO_4^{3-} and OH^- functional groups. It also had pretty favourable crystallographic parameters, and the particle size distribution looked consistent, like a coherent pattern, with a mean particle size of 96.61 μm, and D50 of 101.10 μm. From the SEM and PSA observations, it seems that the micrometre-scale particles were mostly made up of agglomerated calcium phosphate particles, formed during the drying, and then again during calcination. Overall, these results point to the idea that 9 h of post-synthesis calcination created a suitable thermal context which helped with particle growth, crystallographic development, and microstructural organization.

The results seem to back up the potential use of *Pinctada maxima* shell waste as a sustainable calcium supplier, for making biphasic calcium phosphate powders. This route also supports the valorization of marine biowaste, and it lays groundwork for turning shell-derived bioceramics into bone substitute options. That said, the work we have right now is still mostly confined to physicochemical and morphological checkups, not much more. We did not quantify the HAp:β-TCP phase fractions, and as of yet there is not any biological or mechanical performance validation either. So, Sample C should be seen as a promising physicochemical candidate, not a clinically validated bone substitute, at least not based on these data. In future studies, it would be important to do quantitative phase analysis, for example by using Rietveld refinement or the reference intensity ratio method, so you can actually get the HAp and β-TCP weight fractions right. After that, you should also compare the results with commercial or synthetic HAp/β-TCP benchmarks, and not stop there. *In vitro* tests covering bioactivity, cytocompatibility, degradation behavior, mechanical performance, plus *in vivo* evaluations, are still needed to really verify if this material is suitable for bone repair and regeneration type applications.

ACKNOWLEDGEMENTS

This research was funded by the Ministry of Research and Technology (Kemenristek) under the 2025 Penelitian Fundamental Reguler Number: 4403/UN18.L1/PP/2025. We express gratitude for the financial assistance that facilitated the successful completion of this research.

REFERENCES

Ahmad, N. & Elkilania, N. 2022. Association of DEXA with EDX in evaluation of inorganic bone components after application of nano bone for repair of bone defect. *Al-Azhar Assiut Dental Journal* 5(2): 177-191.

Ardiansyah, A., Saraswaty, V. & Risdian, C. 2023. Synthesis and characterization of calcium phosphate (tricalcium phosphate/calcium pyrophosphate) from snail shells (*Achatina fulica*). *IOP Conference Series: Earth and Environmental Science* 1201(1): 012091.

Borštnar, M., Lengauer, C.L. & Dolenec, S. 2021. Quantitative *in situ* x-ray diffraction analysis of early hydration of belite-calcium sulfoaluminate cement at various defined temperatures. *Minerals* 11(3): 297.

Carvalho, G.K., Farias, J.R.S., Lima, I.S., Nascimento, A.M., Neves, G.A., Menezes, R., Osajima, J.A., Braga, A. & Silva-Filho, E.C. 2022. HAp/β-TCP biphasic ceramics obtained by the Pechini method: An antibacterial approach. *Minerals* 12(12): 1482.

Chu, K-T., Ou, S-F., Chen, S-Y., Chiou, S-Y., Chou, H-H. & Ou, K-L. 2013. Research of phase transformation induced biodegradable properties on hydroxyapatite and tricalcium phosphate based bioceramic. *Ceramics International* 39(2): 1455-1462.

Dermawan, S.K., Mohd Ismail, Z.M., Jaffri, M.Z. & Abdullah, H. 2022. Effect of the calcination temperature on the properties of hydroxyapatite from black tilapia fish bone. *Journal of Physics: Conference Series* 2169(1): 012034.

Dinatha, I.K.H., Jamilludin, M.A., Supii, A.I., Wihadmadyatami, H., Partini, J. & Yusuf, Y. 2023. Characteristics of bioceramic hydroxyapatite based on sand lobster shells (*Panulirus homarus*) as sources of calcium with optimal calcination temperature. *Materials Science Forum* 1090: 39-44.

Döbelin, N. 2015. Interlaboratory study on the quantification of calcium phosphate phases by Rietveld refinement. *Powder Diffraction* 30(3): 231-241.

Duta, L., Dorcioman, G. & Grumezescu, V. 2021. A review on biphasic calcium phosphate materials derived from fish discards. *Nanomaterials* 11(11): 2856. https://doi.org/10.3390/nano11112856

Ebrahimi, M., Botelho, M.G. & Dorozhkin, S.V. 2017. Biphasic calcium phosphates bioceramics (HA/TCP): Concept, physicochemical properties and the impact of standardization of study protocols in biomaterials research. *Materials Science and Engineering C* 71: 1293-1312.

Espanol, M., Davis, E., Meslet, E., Mestres, G., Montufar, E.B. & Ginebra, M.P. 2023. Effect of moisture on the reactivity of alpha-tricalcium phosphate. *Ceramics International* 49(11): 18228-18237.

Farzadi, A., Solati-Hashjin, M., Bakhshi, F. & Aminian, A. 2011. Synthesis and characterization of hydroxyapatite/β-tricalcium phosphate nanocomposites using microwave irradiation. *Ceramics International* 37(1): 65-71.

Feng, C., Wu, Y., Cao, Q., Li, X., Zhu, X. & Zhang, X. 2021. Effect of hydrothermal media on the *in-situ* whisker growth on biphasic calcium phosphate ceramics. *International Journal of Nanomedicine* 16: 147-159. https://doi.org/10.2147/ijn.S280130

Firdaus, F.E., Wahfiudin, M.I. & Aprilianti, R. 2022. Utilization of environmental wastes from poultry eggshell to manufacture hydroxyapatite for dental biomaterial. *Proceedings of the International Conference on Industrial Engineering and Operations Management.* pp. 1482-1491.

Ftiti, S., Cifuentes, S.C., Guidara, A., Rams, J., Tounsi, H. & Fernández-Blázquez, J.P. 2024. The structural, thermal and morphological characterization of polylactic acid/B-tricalcium phosphate (PLA/B-TCP) composites upon immersion in SBF: A comprehensive analysis. *Polymers* 16(5): 719.

Fujioka-Kobayashi, M., Katagiri, H., Lang, N.P., Imber, J.C., Schaller, B. & Saulacic, N. 2022. Addition of synthetic biomaterials to deproteinized bovine bone mineral (DBBM) for bone augmentation - A preclinical *in vivo* study. *International Journal of Molecular Sciences* 23(18): 10516.

Ishtiaque, M.S., Das, H., Hoque, S.M. & Choudhury, S. 2022. Synthesis of n-HAP using different precursors and dependence of Vickers hardness on the structure by tuning sintering temperature. *International Journal of Applied Ceramic Technology* 19(3): 1281-1292.

Italiano, A.E.V., Tranquilin, R.L., Marin, D.O.M., dos Santos, M.L. & Vaz, L.G. 2024. Synthesis of calcium phosphate by microwave hydrothermal method. *International Journal of Biomaterials* 2024: 2167066.

Kristianto, N.A., Sari, M. & Yusuf, Y. 2022. Hydroxyapatite based on abalone mussel shells coating on titanium alloy using electrophoretic deposition dip coating as a bone implant candidate. *Chiang Mai University Journal of Natural Sciences* 21(2): e2022021.

Lang, K.N., Lang, N.P., Muños Guzon, F.M. & Saulacic, N. 2025. Bi-layered biphasic calcium phosphate bone substitute to improve bone formation in lateral jaw defects applying the principle of guided bone regeneration: A pre-clinical randomized controlled study. *Clinical Oral Implants Research* 36(9): 1115-1125.

Liu, Y-C., Lee, Y-T., Huang, T-C., Lin, G-S., Chen, Y-W., Lee, B-S. & Tung, K-L. 2021. *In vitro* bioactivity and antibacterial activity of strontium-, magnesium-, and zinc-multidoped hydroxyapatite porous coatings applied via atmospheric plasma spraying. *ACS Applied Bio Materials* 4(3): 2523-2533.

LeGeros, R.Z., Lin, S., Rohanizadeh, R., Mijares, D. & LeGeros, J.P. 2003. Biphasic calcium phosphate bioceramics: Preparation, properties and applications. *Journal of Materials Science: Materials in Medicine* 14(3): 201-209.

Minh, N.N. 2021. Synthesis of biphasic calcium phosphate minerals from shells of poker-chip venus. *Ceramics - Silikaty* 65(3): 281-284.

Mohd Pu'ad, N.A.S., Latif, A.F.A., Ramli, N.D., Muhamad, M.S., Abdullah, H.Z., Idris, M.I. & Lee, T.C. 2020. Extraction of biological hydroxyapatite from bovine bone for biomedical applications. *Materials Science Forum* 1010: 579-583.

Moreira Filho, O., Wykrota, F.H.L. & Lobo, S.E. 2021. Restoring facial contour and harmony using biphasic calcium phosphate bioceramics. *Plastic and Reconstructive Surgery - Global Open* 9(4): e3516.

Muntean, F.L., Olariu, I., Marian, D., Olariu, T., Petrescu, E.L., Olariu, T. & Drăghici, G.A. 2024. Hydroxyapatite from mollusk shells: Characteristics, production, and potential applications in dentistry. *Dentistry Journal* 12(12): 409.

Mustaffa, R., Mohd Yusof, M.R. & Abdullah, Y. 2015. A novelty of synthetic hydroxyapatite from cockle shell and characterization. *Advanced Materials Research* 1087: 429-433.

Ningsih, H.S., Tannesia, L., Chen, H.H. & Shih, S.J. 2021. Fabrication, characterization and *in vitro* cytotoxicity of mesoporous β-tricalcium phosphate using the spray drying method. *Crystals* 11(3): 252.

Putkham, A., Ladhan, S. & Putkham, A.I. 2020. Changing of particle size and pore structures of calcium oxide during calcinations of industrial eggshell waste. *Materials Science Forum* 998: 90-95.

Rahayu, S., Kurniawidi, D.W. & Gani, A. 2018. Pemanfaatan limbah cangkang kerang mutiara (*Pinctada maxima*) sebagai sumber hidroksiapatit. *Jurnal Pendidikan Fisika dan Teknologi* 4(2): 226-231.

Satish, P., Salian, A., Hadagalli, K. & Mandal, S. 2023. Preparation and structural characteristics of biphasic calcium phosphates from prawn shell bio-waste. *Advances in Applied Ceramics: Structural, Functional and Bioceramics* 122(2): 69-78. https://doi.org/10.1080/17436753.2023.2231701

Saulacic, N., Fujioka-Kobayashi, M., Kimura, Y., Bracher, A.I., Zihlmann, C. & Lang, N.P. 2021. The effect of synthetic bone graft substitutes on bone formation in rabbit calvarial defects. *Journal of Materials Science: Materials in Medicine* 32(1): 14.

Shigemitsu, Y., Nagashima, H., Matsunari, H. & Aizawa, M. 2022. *In vivo* evaluation of calcium-phosphate ceramics with highly-interconnected pores using porcine tibia defect model. *Solid State Phenomena* 340: 113-117.

Skliarenko, Y., Kolomiiets, V.V., Balatskyi, V.V., Galuza, Y., Koryak, O.S., Macewicz, L.L., Ruban, T.P., Firstov, S.A., Ulianchych, N.V. & Piven, O.O. 2024. The impact of the physicochemical properties of calcium phosphate ceramics on biocompatibility and osteogenic differentiation of mesenchymal stem cells. *BMC Research Notes* 17(1): 295.

Tran, D.L., Ta, Q.T.H., Tran, M.H., Nguyen, T.M.H., Le, N.T.T., Nguyen Hong, A.P., Park, H-J., Park, K.D. & Nguyen, D.H. 2025. Optimized synthesis of biphasic calcium phosphate: Enhancing bone regeneration with a tailored β-tricalcium phosphate/hydroxyapatite ratio. *Biomaterials Science* 13(4): 969-979. https://doi.org/10.1039/d4bm01179a

Valadão Cardoso, A. & Novaes Ferreira, R. 2024. Dissolution of phosphate and precipitation of carbonate in the biomineralization of the bivalve shell *Limnoperna fortunei. bioRxiv*. doi: https://doi.org/10.1101/2024.05.30.596625

Wang, R., Zhao, D. & Wang, Y. 2021. Characterization of elemental distribution across human dentin-enamel junction by scanning electron microscopy with energy-dispersive X-ray spectroscopy. *Microscopy Research and Technique* 84(5): 881-890.

Weinand, W.R., Cruz, J.A., Medina, A.N., Lima, W.M., Sato, F., Da Silva Palacios, R., Gibin, M.S., Volnistem, E.A., Rosso, J.M., Santos, I.A., Rohling, J.H., Bento, A.C., Baesso, M.L., Da Silva, C.G., Dos Santos, E.X., Scatolim, D.B., Gavazzoni, A., Queiroz, A.F., Companhoni, M.V.P., Nakamura, T.U., Hernandez, L., Bonadio, T.G.M. & Miranda, L.C.M. 2022. Dynamics of the natural genesis of B-TCP/HAp phases in postnatal fishbones towards gold standard biocomposites for bone regeneration. *Spectrochimica Acta - Part A: Molecular and Biomolecular Spectroscopy* 279: 121407. https://doi.org/10.1016/j.saa.2022.121407

Widyastuti, D.A. & Yusuf, Y. 2024. The effect of power rate microwave heating on limestone carbonated hydroxyapatite scaffold using gas foaming method. *Advanced Materials Research* 1179: 11-18.

Wu, S.C., Hsu, H.C., Hsu, S.K., Tseng, C.P. & Ho, W.F. 2017. Preparation and characterization of hydroxyapatite synthesized from oyster shell powders. *Advanced Powder Technology* 28(4): 1154-1158.

Yanti, P.H. & Resmalina, R. 2021. Facile chemical processing of *Geloina coaxans* shell and sodium dihydrogen phosphate as precursors to produce hydroxyapatite. *Jurnal Kimia Valensi* 6(2): 192-197.

*Corresponding author; email: taufik.unram@gmail.com